J. Fluid Mech. (1970), *vol.* 44, *part* 4, *pp.* 661–672
Printed in Great Britain

The oscillatory motions of Rayleigh convection

By G. E. WILLIS AND J. W. DEARDORFF
National Center for Atmospheric Research, Boulder, Colorado

(Received 17 February 1970)

Photographs and simultaneous temperature measurements show that the thermal oscillations which occur in air between horizontal plates with unstable stratification are associated with lateral oscillations of wavy convection rolls. The phenomenon appears to consist of an oscillating motion nearly independent of depth superimposed upon the convective motions, and is best viewed from above. For large Prandtl number the photographic evidence suggests that the first unsteady motions to occur consist of a very similar oscillation, except that the features which oscillate are updraft and downdraft lines of short length. The periods of the oscillations obtained visually agree well with those reported previously from fixed temperature measurements, and a weak oscillation of doubled frequency is explained.

1. Introduction

Thermal oscillations in Rayleigh convection which precede the occurrence of turbulent motions have been reported by Willis & Deardorff (1965, 1967), Rossby (1966), and Krishnamurti (1970). The periods of the oscillations have been fairly well established for a wide variety of fluids and fluid conditions. Still, there is much uncertainty about their proper interpretation and the nature of the causal mechanism.

The period of the oscillation agrees rather well with a theory for large Rayleigh-number convection developed by Howard (1966), and this led Rossby (1966) and Willis & Deardorff (1967) to suggest they could be explained by this theory. It is a mechanistic theory in which the boundary layer is assumed to become unstable, causing thermals to be released which effectively wipe out the boundary layer. The latter then grows back by purely molecular diffusion of heat until it again becomes unstable, and the resulting periodicity of the process can be calculated to depend upon $R^{-\frac{2}{3}}$, where R is the Rayleigh number.

A different explanation was invoked by Krishnamurti (1970) who, on the basis of temperature measurements and photographs displaying a lineal-time representation of the flow, associated the oscillations with circulating spots of relatively warm or cool fluid to which the theory of Welander (1967) is applicable.

In an unreported study the present authors noted several inconsistencies between the observed temperature oscillations and expected behaviour from a model consisting either of thermals breaking away from a boundary or of temperature anomalies circulating around the periphery of a convective vortex.

The most serious discrepancy was determined from measuring oscillations in air with a vertical array of temperature sensors. Rather than observing systematic phase shifts in temperature which a thermal or hot/cold spot would display as it moved from the region of one sensor to the next, we noticed that the oscillations appeared to be closely in phase in the vertical. These measurements indicated that there were thermal oscillations occurring within the fluid which were nearly independent of depth.

Also, we have viewed a time-lapse movie reported by Rossby (1966) in which oscillations apparently extending throughout the fluid depth are clearly visible from a top view. The fluid was a silicone oil of Prandtl number 100. However, Rossby did not associate them with the thermal oscillations.

To gain more information about the oscillations it was felt that further direct visual observations would be essential. A top view is optimum from which to view oscillations that are nearly independent of depth. However, it is generally difficult to maintain the desired upper boundary condition of constant temperature when using a glass plate as the upper boundary. For this reason, we have utilized only two fluids in this study, namely air and silicone oil, which have relatively small thermal conductivities in comparison with glass. In order that the glass plate temperature be sufficiently uniform, the ratio

$$\frac{\Delta T_g}{\Delta T} = \frac{\delta k}{h k_g} N$$

should be considerably less than unity, where ΔT_g is the temperature drop across the glass plate, ΔT the drop across the working fluid being investigated, δ the thickness of the glass, h the depth of the working fluid, k the thermal conductivity of the working fluid, k_g that of the glass, and N the Nusselt number. For our convection chamber (to be described in §2) and for the Rayleigh numbers employed, this ratio was about 0·2 for silicone oil and about 7×10^{-3} for air. The latter ratio is certainly sufficiently small, and evidence to be presented later indicates that the former was also, for purposes of this study.

There have been previous top-view observations of convection in air by Chandra (1938). Although his study was restricted to Rayleigh numbers too close to the critical for the oscillations to occur, he demonstrated that smoke could be used satisfactorily as a tracer in air. In our study an oil smoke is used as the tracer in air, and graphite particles similar in size and shape to aluminium pigment are used as flow tracers in the silicone oil.

2. Description of equipment and experiments

The convection chamber, schematically depicted in figure 1, has for the lower boundary a square aluminium plate of thickness 1·9 cm and length 80 cm, and for the upper boundary a glass plate of the same horizontal dimensions and thickness 0·32 cm. Variations in fluid depth h were minimized by using 15 plastic spacers of 0·63 cm diameter to support the glass plate. The surface of the aluminium plate was painted flat black for improved photographic contrast. The side walls consist of plexiglass of thickness 1·27 cm. Heat was applied

to the lower boundary by the use of a thin electrical heat-flux pad resting upon a second aluminium plate. The upper boundary temperature was maintained nearly constant by circulating cool water above the glass plate, with inlets at the four corners and outlet at the centre. A horizontal plexiglass plate was placed just above and in contact with the water bath to provide a ripple-free upper surface, and to provide supports for the water inlets and outlet. The average boundary temperature difference across the working fluid, ΔT, was

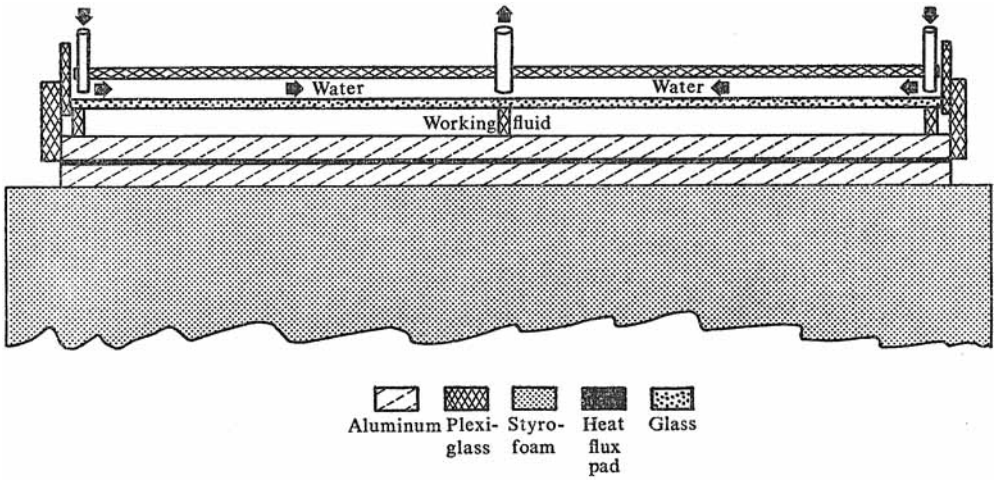

FIGURE 1. Schematic drawing of convection chamber, side view. The length of a side is 80 cm.

Fluid	α (C^{-1})	ν (cm^2 sec^{-1})	κ (cm^2 sec^{-1})	h (cm)	σ
Air	$3{\cdot}38 \times 10^{-3}$	0·194	0·272	2·54	0·71
Silicone oil	$1{\cdot}05 \times 10^{-3}$	0·050	$8{\cdot}77 \times 10^{-4}$	1·05	57

TABLE 1

measured with thermocouples located in the aluminium plate and near the water outlet on the upper surface of the glass plate. Corrections to ΔT, ranging to a maximum of about 20 %, were made to account for the temperature drop across the glass plate when silicone oil was the working fluid. Average values of the relevant fluid physical properties are listed in table 1, where α is the coefficient of thermal expansion, ν the kinematic viscosity, κ the thermometric conductivity, and σ the Prandtl number.

Several aspects of the requirement of uniform boundary conditions were checked preliminary to the experiments in silicone oil. Excluding regions within 2 cm of the sidewalls, it was found that maximum horizontal variations in lower boundary mean temperature were about 1 % of ΔT; while the maximum temperature variation in the circulating water above the upper boundary was 3 % of ΔT. Horizontal variations in depth, due mainly to sag of the glass plate, were less than 2 % of the depth h in the case of the silicone oil and less than 1 % in the

case of air. Thus, horizontal variations in $R = (g\alpha\Delta T h^3)/(\nu\kappa)$ are believed to have been under 5–10 %.

Thermocouples of time constant about 0·5 sec in air were used for all temperature measurements within the fluid.

Flow visualization of the convective patterns in air was provided by an oil smoke composed of atomized particles of dioctyl phthalate with average diameter $1{\cdot}5 \times 10^{-4}$ cm and specific gravity about 1. These spherical particles do not, of course, tend to orient with fluid shear, and only the variations in smoke concentration allow the patterns to be observed. While one might expect the smoke concentration to become uniform soon after introduction of the smoke, a 'fallout slit' occurring at the centres of downdrafts allows the convection patterns to be observed when R is not too large. When rolls were the dominant form of convection, Chandra's (1938) photographs also appear to exhibit this feature.

The occurrence of a 'fallout slit' at the downdrafts can be explained by a theory of Calder (1958) for the motions of relatively heavy particles in a rotating fluid. It suffices to state that when the axis of rotation is perpendicular to the gravitational acceleration (which holds essentially for a convective vortex in a horizontal chamber), then the combined effect of gravity and rotation is to translate the particle horizontally a small distance from the axis of rotation and to suppress its fallout. For the conditions used here with smoke particles in air, the predicted translation is about 0·02 cm in a direction from the downdraft towards the updraft. Thus, a region free of smoke of about 0·04 cm width is expected at the downdrafts. This distance is consistent with those observed. The opposite effect occurs at updrafts where there is a slight overlapping of particles from adjacent vortices. However, the increased concentration at the updrafts is not nearly so noticeable as the absence of particles at downdrafts due to the much greater brightness contrast in the latter case. The location of updrafts could generally only be noted when variations in smoke concentration existed between adjacent vortices.

Spheres of oil smoke which fall out present no problem, as they merely form a very thin conducting film on the chamber bottom and cannot be picked up again by the flow.

Both 35 mm still photographs and 16 mm time-lapse movies of the patterns were taken from above with light directed from one side. The somewhat diverging light beam illuminated approximately the upper half to two-thirds of the chamber in the region of photographs.

The experimental technique employed in air was to maintain the desired Rayleigh number constant at least half an hour before introducing the smoke. Then a 4–5 min waiting period was allowed to permit the flow to re-establish itself before photographs were taken in a section of the chamber near the point of introduction of the smoke. Photographs with sufficient contrast could be taken for about 15 min, after which the diffuse smoke would be removed and the above procedure repeated.

In the case of silicone oil, a small quantity (less than 0·02 % of the fluid weight) of graphite particles of about $1{\cdot}5 \times 10^{-3}$ cm average length and with specific

gravity of about 2 were used as the flow tracers. Graphite particles, though less efficient reflectors of light than aluminium particles, were used because of their smaller specific gravity. The particles, having a greater surface area in one plane, tend to align with the fluid shear or to stay aligned by pre-existing shear, so that the blackened chamber bottom is viewable for both updrafts and downdrafts. (Although there is no shear at the centre of an updraft, particles very close to the updraft axis at a given time will have been previously travelling very close to the chamber bottom where the shear is largest. There the alignment is one with the unit vector of the particle area pointing normal to the shear. After the particle moves away from the boundary and into the updraft the unit vector must become horizontal in which case only a thin edge shows from above.) Even with the graphite particles, however, the fallout rate was greater than desired for $\sigma = 57$. Nevertheless, it was possible to gather useful data over a period of several hours by introducing the silicone oil with graphite particles into the chamber after the desired value of ΔT had already been attained. Thus the convective fluid motions which quickly became established prevented undue initial fallout of particles.

3. Experimental results

3.1. *Description of oscillations in air*

The oscillation structure is simplest at low Prandtl number ($\sigma < \sim 1$) because it then appears at a low Rayleigh number for which the horizontal plan form is simplest and consists mainly of rolls. In air, oscillations first appear at

$$R \cong 5800 \cong R'$$

(the critical value for onset), and most of the observations to be reported were made for $9000 < R < 9500$. At these R the oscillations in air occur frequently and with appreciable amplitude.

Measurements in air with thermocouples aligned vertically disclosed that the thermal oscillations are nearly in phase throughout a vertical line, being most closely in phase at points equidistant from mid-chamber level. They are also of comparable amplitude at all heights not too near the boundaries. These results are shown in figure 2, for which the thermocouples were close to, but not at, the axis of an updraft. The skewness of the oscillation observed at $z/h = 0{\cdot}8$ will be discussed later.

Temperature phase differences between levels, which are scarcely detectable in figure 2, have been analyzed for 51 individual oscillations from 6 distinct cases when the thermocouples were relatively near updrafts. We found that near either boundary, at $z/h = 0{\cdot}2$ or $0{\cdot}8$, the thermal phase lags that of the interior by about 10° on the average. Although indirect, these measurements alone suggest that the oscillations consist of a fluid motion which is variable in the horizontal but nearly independent of z, with frictional retardation occurring near the boundaries. Photographic evidence to be presented next supports this conclusion.

Photographs of flow patterns for two cases when oscillations were being recorded by the thermocouples are shown in figure 3, plate 1. The sinusoidal shape of downdraft lines participating in an oscillation is clearly observable for other-

wise straight rolls in figure 3 (*a*) and for curved rolls in figure 3 (*b*). The oscillations seem to be centred about either an updraft or downdraft with equal probability. The fallout slit at the centre of a downdraft, through which the blackened bottom of the chamber is viewed, is usually in evidence throughout the oscillation. This tends to support the thermal evidence that the oscillation consists of a net horizontal motion throughout the chamber depth, superimposed upon the continuous convective motions which lie in vertical planes.

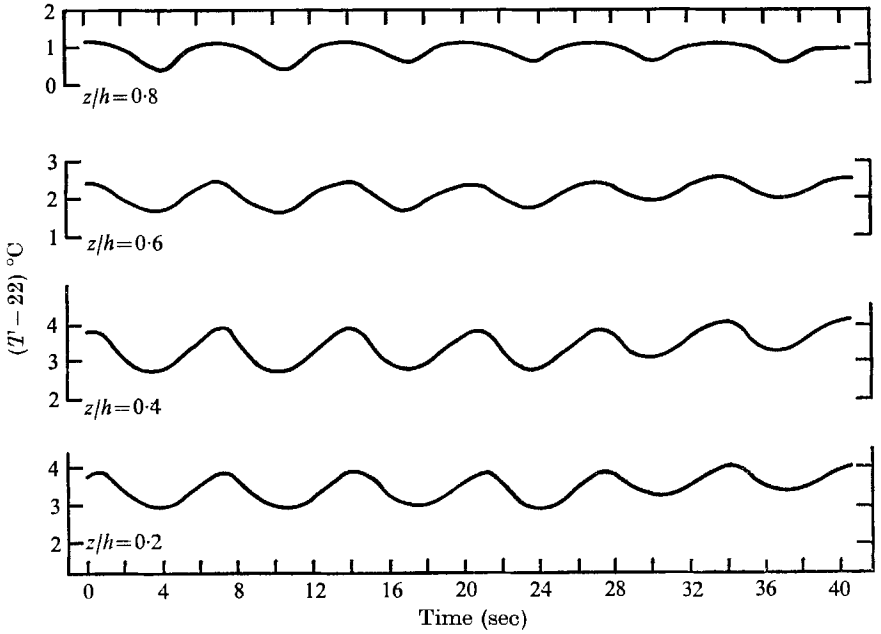

FIGURE 2. Simultaneous temperature records at four levels in air, $R = 9200$.

The ratio of the average wavelength along a sinusoidal roll edge during oscillations to the average distance between downdrafts was found to be approximately 0·7. That is, the typical wavelength of the wavy roll edge is $2{\cdot}5h$ while that of the roll itself is $3{\cdot}5h$ at $R = 9000$.

Unfortunately, we have been unable to determine clearly the upper-half streamline directions, viewed from above, with respect to the phase and propagation direction of a wave. Oil smoke does not lend itself to these purposes.

A side view of rolls which were undergoing oscillations is displayed in figure 4, plate 2. This photograph and time-lapse movies taken from this viewpoint help confirm that a roll edge remains close to the vertical during oscillations.† However, from this view the fallout slit was generally not visible and the precise location of the downdraft axis could not be determined.

A temperature cross-section in a vertical plane containing convective vortices undergoing oscillations was measured by quickly moving the vertical array of thermocouples through the fluid in a horizontal arc of radius 13 cm. With the sensor movement (about 3 cm/sec) being several times faster than the propagation speed of the oscillation, the approximate result is an x'-z representation of the

† Subsequent side views showed that roll-edge tilt angles of up to $\pm 10°$ could occur.

temperature, where x' is the distance along the arc. The temperatures were corrected both in amplitude and phase from knowledge of the thermocouple time constant. A photograph of the downdraft lines $\frac{1}{2}$ sec before initiation of sensor movement is shown in figure 5(*a*), plate 3. The drawing of the boundary gradients in the cross-section of figure 5(*b*) was aided by knowledge of the average Nusselt number of 2·4 for this R of 9200.

In figure 5(*b*) both temperature extremes, corresponding to the downdraft and updraft near the interior of the arc in 5(*a*), are seen to be vertically oriented while undergoing oscillations. However, at mid-chamber level there was a stronger horizontal temperature gradient on the left-hand side of the downdraft than on the right. Also, the updraft to the right appears broader in horizontal extent than the downdraft on its left. The latter feature is probably caused by the direction of sensor travel becoming somewhat non-perpendicular to the length of the rolls towards the right-hand side of the arc. There is a slight bulging of the isotherms near the downdraft at $x'/h = 2{\cdot}5$ and $z/h = 0{\cdot}5$ which is unexplained. Although oscillations were definitely occurring during the measurement of this cross-section, the isotherm pattern gives no indication of thermals leaving the boundary or of temperature anomalies travelling around the periphery of the vortex.

With the aid of figure 5(*b*), the skewness in the thermal oscillation of figure 2 at $z/h = 0{\cdot}8$ can be given a plausible explanation. A lateral amplitude for the oscillation of $\Delta x'/h = 0{\cdot}6$ would produce, for the isotherms of figure 6(*b*), plate 4, and for thermocouples located at $x'/h = 3{\cdot}3$, thermal oscillations of the approximate amplitude observed in figure 2. A simplified picture is that the fluctuations there are roughly equivalent to moving the thermocouple array horizontally in a fixed isotherm field like 5(*b*) for $3{\cdot}0 \leqslant x'/h \leqslant 3{\cdot}6$. Due to the broad, flattened isotherm structure near the top of the updraft, the temperature at $z/h = 0{\cdot}8$ would be nearly uniform for $3{\cdot}4 \leqslant x'/h \leqslant 3{\cdot}6$ which would correspond to the flat portions of the cycles in figure 2 at $z/h = 0{\cdot}8$.

A combined photographic and temperature-measurement experiment was also performed with stationary thermocouples near chamber mid-level. Values of the distance of the thermocouple sensor from the nearest downdraft axis, measured in a direction normal to that of the average roll length, are plotted atop the simultaneous temperature recorded in figure 6(*a*). A direct distance–temperature correspondence is noted.

It is noted that the temperature fluctuation at a point could be associated either with a standing wave motion of the roll, with a translation or propagation of the wave shape, and/or with development or decay. Usually some combination occurs, though in the case of figure 6, propagation from left to right was the dominant event. The average wave propagation speed for this case was 1·2 cm sec^{-1} or about one-third of the estimated maximum vortex flow speed.

This type of analysis was extended for several oscillation periods and is shown in figure 7. The thermocouple location was about midway between updraft and downdraft with oscillations at both roll edges being approximately in phase. A very good correlation is evident between $T'/\Delta T$ and d/h, again implying that the thermal oscillation is only a result of the lateral displacements of the temperature field.

Continuous temperature measurements at a point for a data period of about 9 min are shown in figure 8. Visual observations confirmed that the rolls were migrating (with time scale on the order of minutes) and that the temperature sensor was close to a downdraft from 0 to 1·2 min and 7·2 to 8·2 min; and close to an updraft from 2·0 to 4·2 min, 5·6 to 6·8 min, and 8·5 to 8·9 min. During the remaining periods the thermocouple was located more nearly intermediate between updrafts and downdrafts. Now, if a thermocouple happens to be situated outside the range of oscillation of a roll edge, which is the usual case for small-amplitude oscillations, the period measured will coincide with that observed visually. However, if it is situated within the range of oscillation of the roll edge, clearly the frequency on a temperature record would be twice that of the

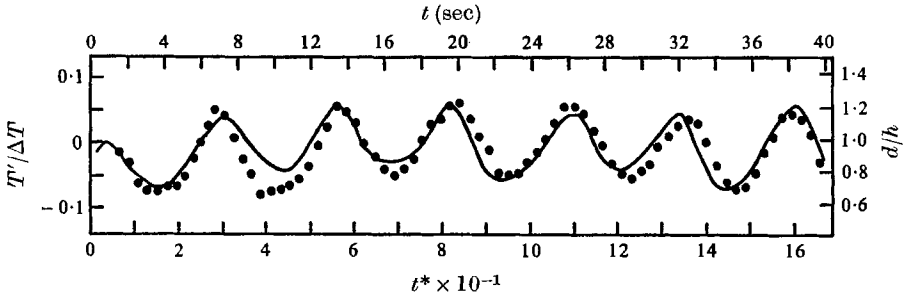

FIGURE 7. Record of temperature fluctuation relative to ΔT as a function of time (solid curve with abscissa on left), along with values of the relative distance d/h (black dots with abscissa scale on right) of the sensor from the nearest downdraft axis. t^* is the dimensionless time $(k/h^2)t$.

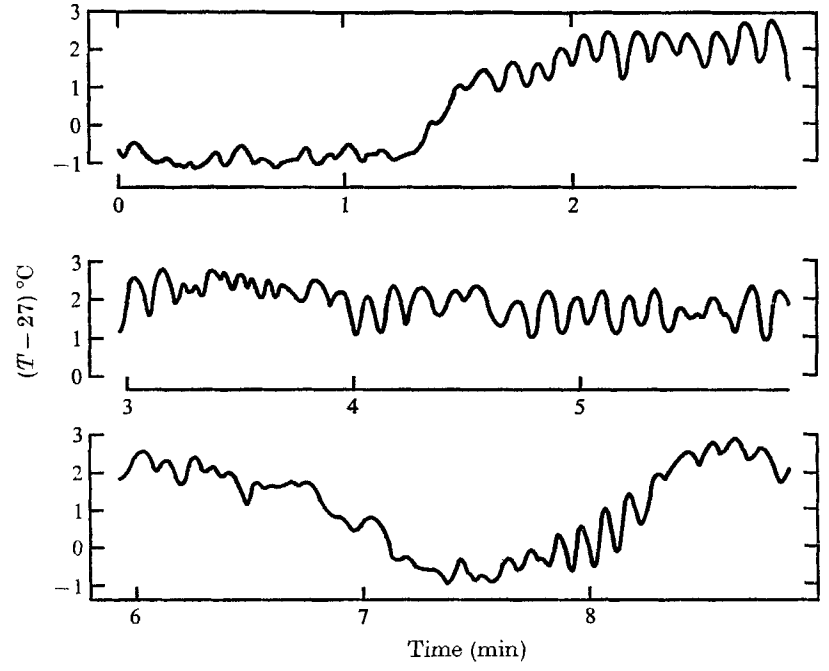

FIGURE 8. Temperature in air at the height $z/h = 0{\cdot}8$, as a function of time. $R = 10{,}800$.

movement of the roll edge. Examples of such occurrences are to be seen in figure 8 at a downdraft for times 0·4 to 1·2 min, and at an updraft for times 3·2 to 3·8 min and 6·2 to 6·7 min. The movement of the roll edge across the thermocouple at these times was verified visually. The amplitude in the region of doubled frequency is relatively small because the temperature extrema are not sharp at small R (see figure 5(*b*)). This phenomenon may explain four data points of Rossby (1966) which show about half the expected period. Oscillations of doubled frequency have also been reported by Krishnamurti (1970), who attributed them to the circulation of two warm or cold anomalies within the same convective vortex.

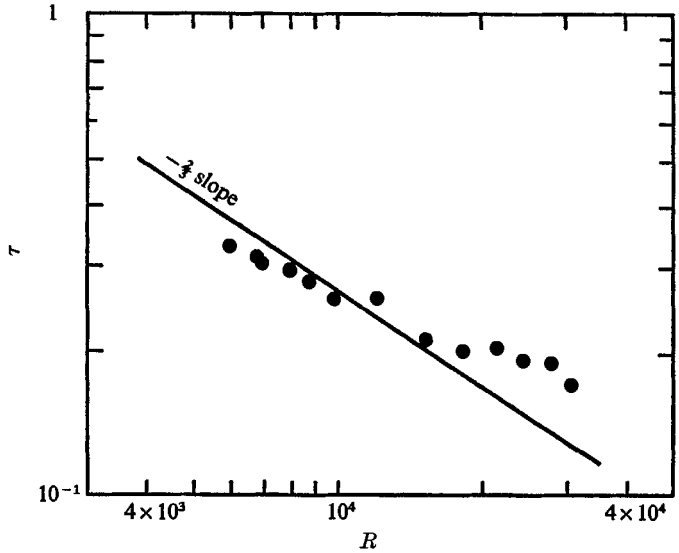

FIGURE 9. Plot of dimensionless thermal oscillation period τ *versus* Rayleigh number R in air.

From measurements at several values of R the average dimensionless periods of the oscillations were determined. Only the most clearly sinusoidal temperature fluctuations were considered in the analysis, with the doubled frequency being excluded. The results are shown in figure 9, where τ is the period made dimensionless by h^2/κ. Standard deviations of τ have been calculated for several R with the results: $R = 8740$, $\tau = 0{\cdot}278 \pm 0{\cdot}042$; $R = 12{,}100$, $\tau = 0{\cdot}256 \pm 0{\cdot}060$; and $R = 30{,}700$, $\tau = 0{\cdot}170 \pm 0{\cdot}034$. These values illustrate that a fairly broad range of frequencies is present for any fixed R even when only the most sinusoidal oscillations are considered. The $-\frac{2}{3}$ slope line predicted by Howard for the boundary-layer redevelopment time at high Rayleigh number is not a good fit to the data; a $-0{\cdot}4$ slope would fit better. Yet it is clear from Rossby's (1966) figure 4.1 and Krishnamurti's (1970) figure 20 that if fluids of various σ are utilized and the periods determined over several decades of R, the $-\frac{2}{3}$ slope is a good overall fit. Therefore there appears to be a dependence upon σ which is in the sense of a decreased period for increased σ. A tentative relationship which brings our periods for air into agreement with Krishnamurti's (1970) average basic period for water is $\tau = 9{\cdot}6R^{-0{\cdot}4}\sigma^{-0{\cdot}4}$.

However, a modified relationship probably holds for $\sigma > \sim 10$, with decreased σ dependence and increased R dependence.

When R reaches about 12,000 we estimate visually that the oscillations occur essentially all the time over most of the area. This R agrees well with the value of about 11,000 found by Willis & Deardorff (1967) for an intermittency factor 'I' first reaching unity ('I' = 1 means 'always occurring'). The only roll edges which appear to be nearly immune to the oscillations are those which are strongly curved, as in a small closed cell or a doughnut-shaped roll.

The amplitude of the oscillations was observed to increase rapidly with R for $R' < R < \sim 8000$. Above $R \cong 8000$ very little further increase was noted, although wave breaking was occasionally observed for $R > \sim 12{,}000$. In this case, fluid at the crests within the oscillating roll spills into the next adjacent roll of like vorticity.

Another interesting feature to be observed as R is increased beyond about 12,000 is the greater prevalence of short length, isolated sharp-crested waves. This feature develops quickly and travels along a roll edge for only a relatively short time before breaking up or losing its identity.

The above two processes, and others to be mentioned, cause the convection to be sufficiently turbulent in appearance, for $R > 30{,}000$ in air, that well-defined thermal oscillations at a given point are rarely discernible.

Two other time-dependent phenomena were observed in air for R less than 3000 as well as for larger R. In regions where the rolls are strongly curved (which occur even within a rectangular convection chamber), it seems that the roll or cell diameter often becomes too large for equilibrium to be maintained. Then a new cell appears as an expanding blob at the region of maximum curvature of a roll edge or in the centre of the larger cell. Invariably the new cell fails to remain symmetrically within the adjacent rolls or larger cell, and migrates to one side where it disturbs neighbouring rolls until a new quasi-steady pattern is obtained. A rather complicated example of this process is shown in figure 10(*a*)–(*f*), plate 6, for $R = 4250$. In addition to the new cell which is centred just to the left of centre in 10(*a*), one forms in the upper right after 10(*b*).

The other phenomenon is the occasional mean drift of fluid at all depths within a roll, or within several adjacent rolls, along the length of the roll(s). When this occurs, the roll is often straighter over a greater length than usual, i.e. more two-dimensional except for the oscillations. It is not clear if the greater two-dimensionality on these occasions is caused by the mean drift, or if development of a mean drift is aided by the presence of straight rolls with oscillations. Mean drift speeds varied from zero to about 50 % of the maximum orbital or convective speed. Mean drift was present for the photograph of figure 3(*a*), with the drift direction being towards the lower edge of the photograph.

Both of these latter two processes occurred for R either greater or smaller than R'. However, they did not necessarily cause initiation of oscillations, which sometimes grew from disturbances too small to detect. We now believe that these two phenomena constituted the long-term non-oscillatory unsteadiness sensed with thermocouples by Willis & Deardorff (1965) and which is also evident in figure 8.

3.2. *Description of oscillations for Prandtl number* 57

Very similar oscillations were also observed in silicone oil with $\sigma = 57$. In this case R' is of order 10^5 and the convective plan form is very complicated. For $R < R'$ the only time-dependence noted was gradual adjustment, over periods of hours rather than minutes, of the locations of recognizable features. At $R = R'$ and for $h = 1{\cdot}05$ cm the oscillations have a period of about 22 sec and thus require, in general, time-lapse photography to discern them. Figure 11, plate 7, is a photograph of the typical structure at $R = 4{\cdot}5 \times 10^5$ for which oscillations were occurring. Because of the use of graphite particles as flow tracers here, both the updraft and downdraft axes appear as dark lines.

Unlike the case of air, the structure which first undergoes oscillations at large R and σ is not a long roll, but is an up- or down-draft segment having one end anchored to a more prominent up- or down-draft and the other end free. The white arrows denoted by (*a*) point out two such features which were definitely oscillating at the time of the photograph, as determined by comparison of several sequential photographs. Several other minor up- and down-draft segments were also undoubtedly oscillating but could not be definitely identified without recourse to a movie of which, however, individual frames were of poorer quality.

The amplitude of the oscillation increases with distance from the anchored end towards the free end, and waves sometimes propagate in that direction. Viewed from above, the convective-flow streamlines directed towards the oscillating line change orientation during the oscillation, but generally form an acute V angle at the up- or down-draft line. This fact contrasts with the right angle between the convective flow plane and the roll edge at the onset of oscillations at small σ. At $\sigma = 57$, a main up- or down-draft line having no free end as denoted, for example, by the white arrow labelled (*b*), does not partake in an oscillation unless R is increased beyond about 4×10^5. Then the oscillation is a standing wave rather than a propagating one.

The dimensionless period τ of these oscillations has been obtained from time-lapse movies we have taken and from the movie of Rossby (1966). The values fit well onto the curve of τ *versus* R obtained from temperature measurements by Krishnamurti (1970) for which the upper boundary was a thick slab of conducting metal. This correspondence suggests these visually observed oscillations are the source of the thermal oscillations, and that the use of a thin glass plate as upper boundary, surmounted by a circulating cool water bath, does provide a sufficiently close approach to constant temperature when studying the oscillations within a silicone oil.

Our top view for $\sigma = 57$ gave no definite indication of thermals or circulating blobs in the fluid, at least for $R < 4{\cdot}5 \times 10^5$. However, occasional sharp-edged bright 'bursts' have been noticed to appear suddenly in restricted regions and to move with the convective flow. A possible explanation appears to be variations in tracer concentration caused by the first movement of an up- or down-draft line which had previously been stationary. This could allow some tracer particles which accumulate on the bottom underneath the line to be set in motion. A thorough search with the simultaneous use of temperature probes

and camera, before tracer fallout had become significant, would be necessary to determine if the bright bursts are instead associated with a different phenomenon such as the circulation of temperature anomalies.

4. Conclusions

Evidence presented in this study shows rather conclusively that oscillations extending coherently throughout the chamber depth occur in air and probably also in silicone oil of Prandtl number 57. Through the use of simultaneous temperature measurements and photographs, the thermal oscillations in air are concluded to be caused by lateral displacements of the updrafts and downdrafts during oscillations of the wavy rolls. The periods of oscillation obtained visually in both air and oil agree with those reported in previous investigations at similar R and σ. The oscillations in silicone oil have the same appearance as in air except that the features which oscillate most readily are up- or down-draft segments of rather short length having one end free.

A theoretical explanation totally different from those previously invoked is needed to explain the favoured roll-edge wavelength at small R and σ, the dependence of R' upon σ, and the velocity structure which permits the roll or cell edges to remain essentially vertical during oscillations. Some recent (unpublished) three-dimensional numerical integrations by F. Lipps (Geophysical Fluid Dynamics Laboratory, ESSA, Princeton University) appear to have reproduced the oscillations and should permit a good understanding of the associated velocity structure. A concurrent linear theory of Lipps suggests that the basic mechanism involves the generation of lateral vorticity (in a vertical plane at right angles to that of the longitudinal vorticity of the basic rolls) caused by the horizontal temperature gradients along the basic roll length associated with waviness. Then vertical vorticity (lying in the horizontal plane) is generated by the tilting of the basic roll vorticity by the lateral vorticity. The lateral component of this horizontal velocity, if oscillatory, would then transport the basic temperature field to produce thermal oscillations as deduced in this study.

The National Center for Atmospheric Research is sponsored by the National Science Foundation.

REFERENCES

CALDER, K. L. 1958 *Technical Study* 13, *Biological Warfare Lab.* Available from ASTIA.

CHANDRA, K. 1938 *Proc. Roy. Soc.* A **164**, 231–42.

HOWARD, L. N. 1966 In *Proceedings of the Eleventh International Congress on Applied Mechanics*, p. 1109–15. Berlin: Springer.

KRISHNAMURTI, R. 1970 *J. Fluid Mech.* **42**, 309.

ROSSBY, T. 1966 *Dept. of Geology and Geophysics M.I.T. Sci. Report* HRF/SR27.

WELANDER, P. 1967 *J. Fluid Mech.* **29**, 17–30.

WILLIS, G. E. & DEARDORFF, J. W. 1965 *Phys. Fluids*, **8**, 225–9.

WILLIS, G. E. & DEARDORFF, J. W. 1967 *Phys. Fluids*, **10**, 931–7.

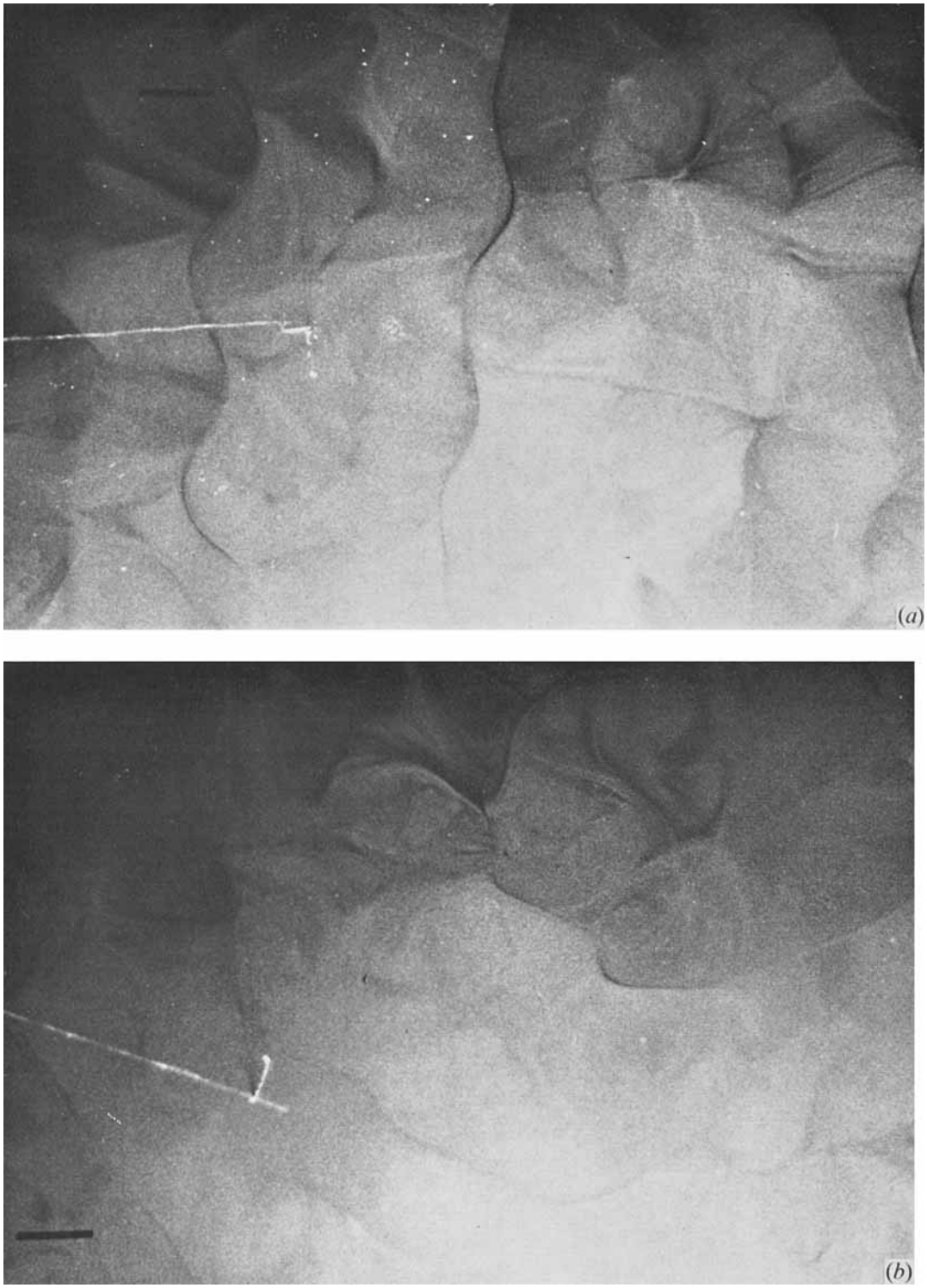

FIGURE 3. Oscillations in air, top view, $R = 9000$. Length of black scale marker is equal to the chamber depth of 2·54 cm. Thin white lines on left are thermocouple lead wires and sensors. (*a*) Nearly straight rolls, (*b*) curved rolls.

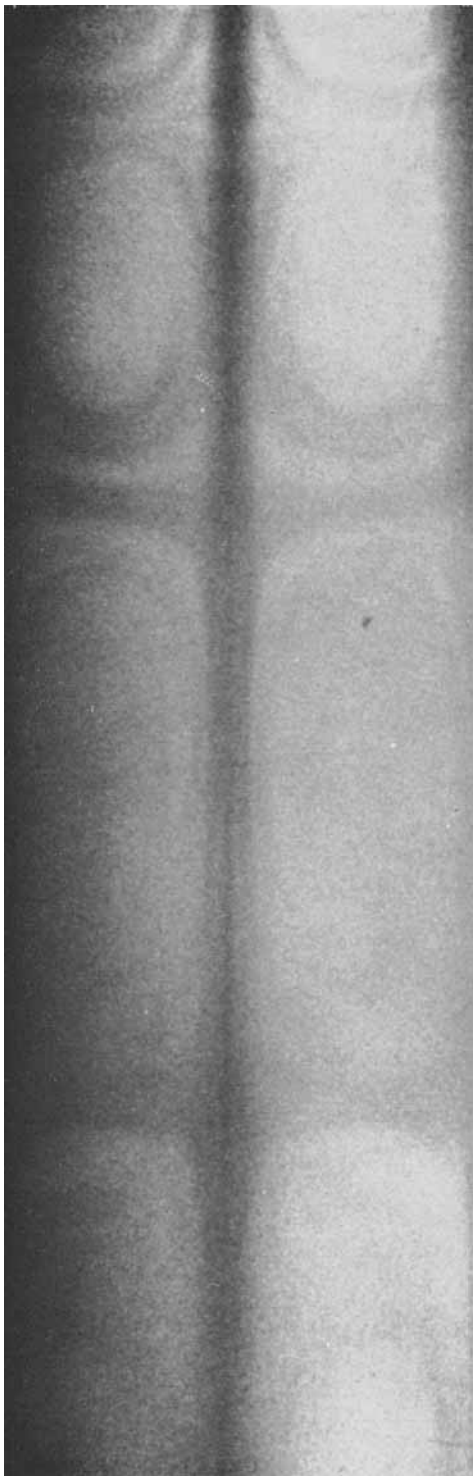

FIGURE 4. Side view of rolls during occurrence of oscillations in air, $R = 9500$. The fluid extends from the lower edge of the photograph to the horizontal line at mid-level; the upper image is a reflexion from the upper glass plate. Faint black streaks are regions of decreased smoke concentration which are nearly parallel to the streamlines.

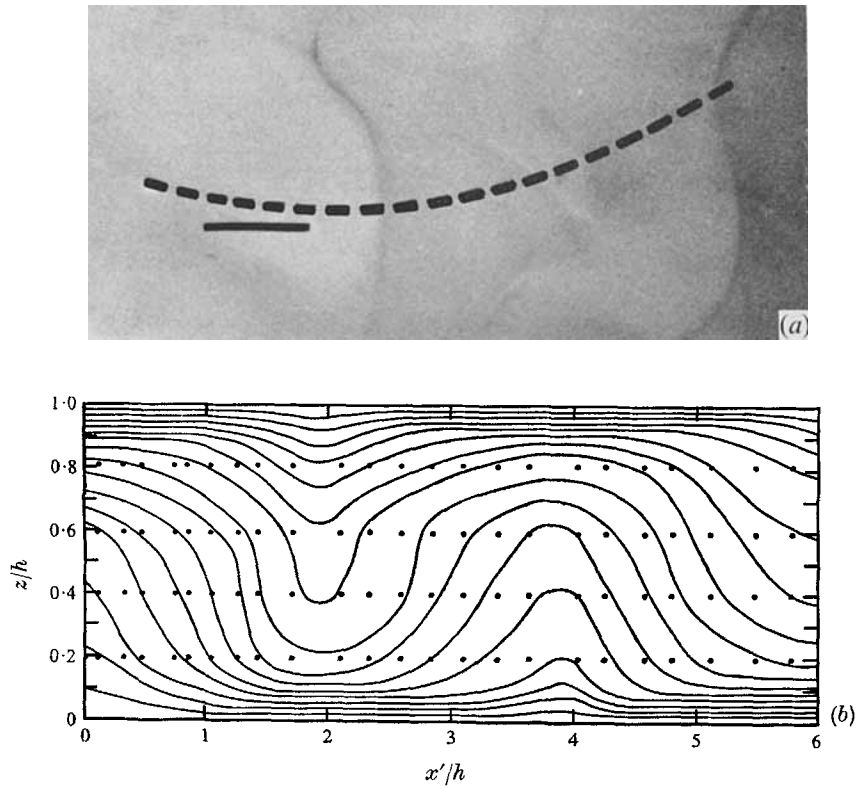

FIGURE 5. (*a*) Top view of wavy convection rolls in air at $R = 9200$, showing the arc (dashed curve) travelled by the vertical array of thermocouples. Travel direction was from left to right. (*b*) Temperature cross-section along the dashed curve in (*a*). Dots indicate points of measurement used in the analysis. Isotherm interval is 0·55 °C. The end points $x'/h = 0$ and 6 correspond to the left and right ends, respectively, of the arc in 5(*a*).

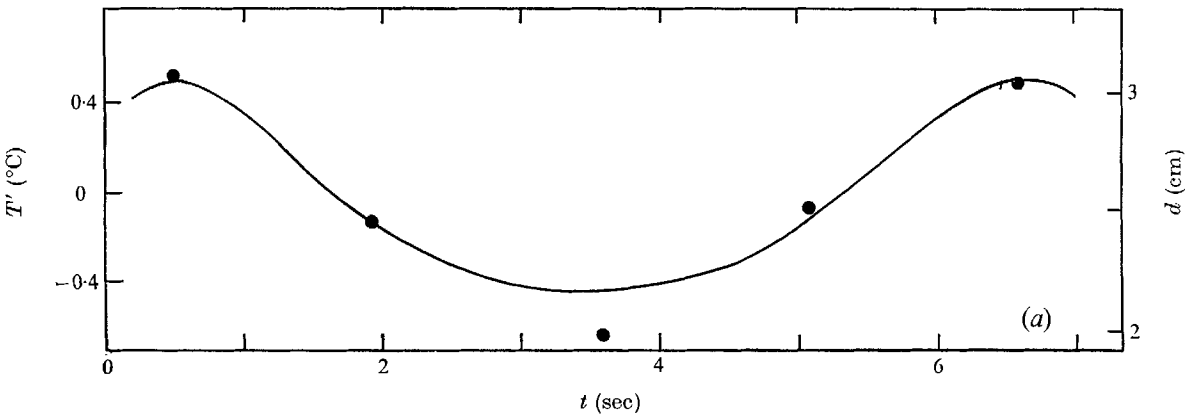

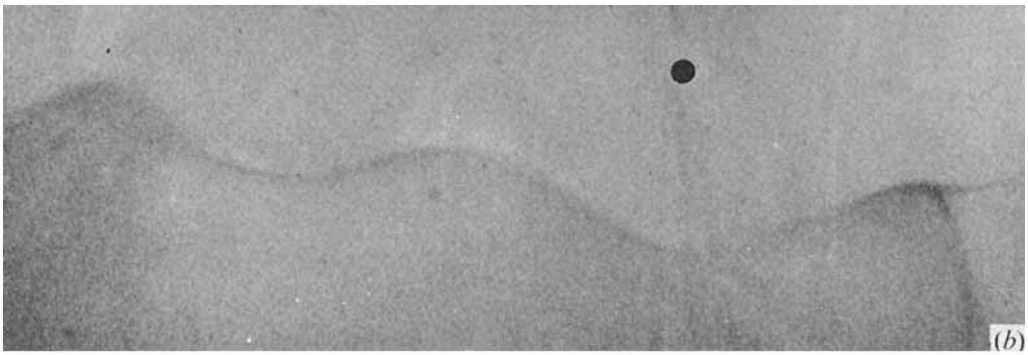

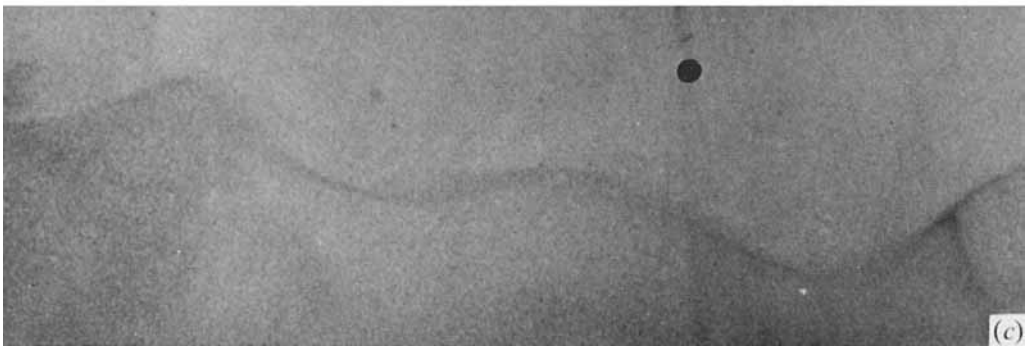

For legend see facing page.

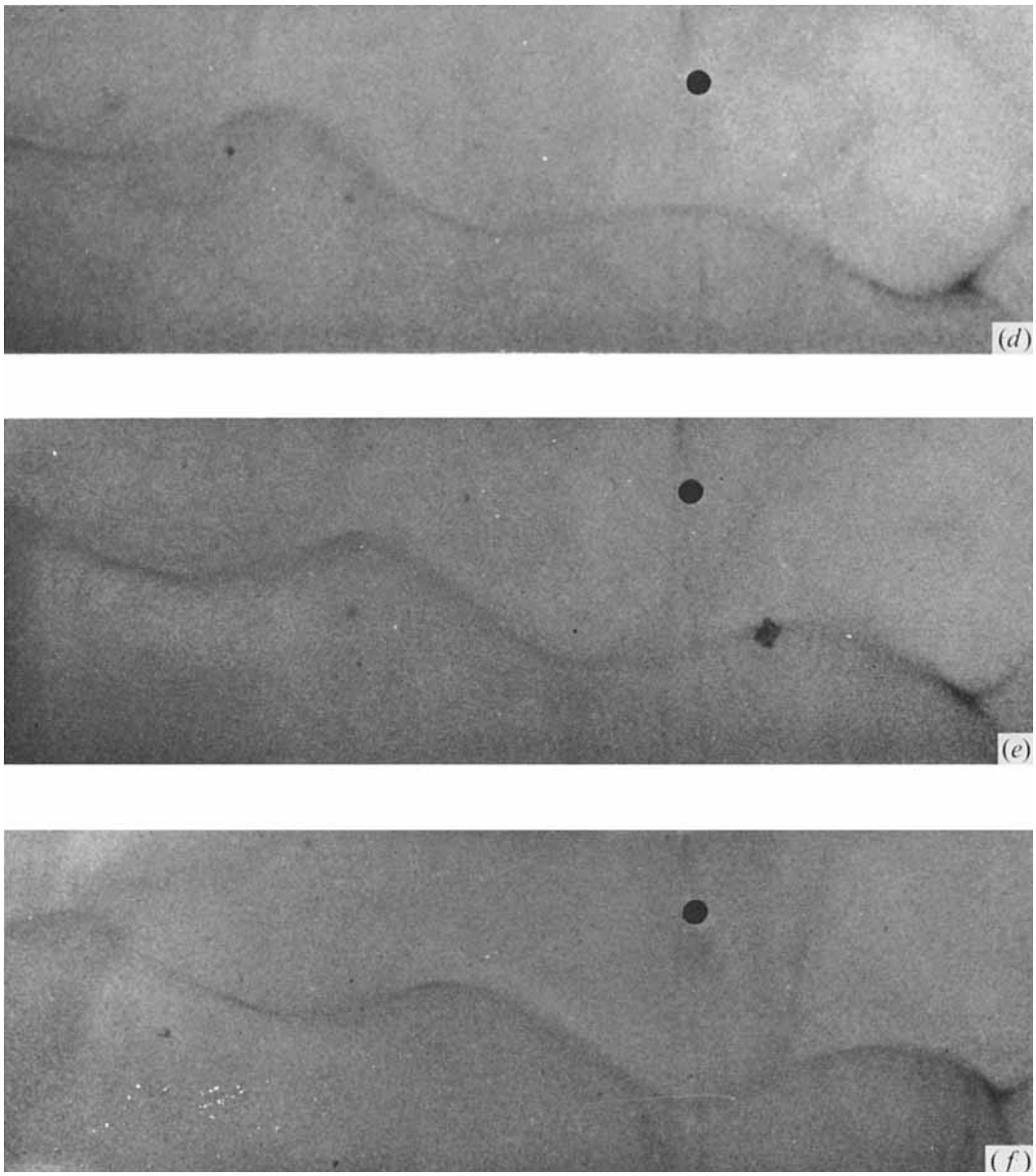

FIGURE 6. (*a*) Temperature trace (solid curve with abscissa scale on left) as a function of time, along with values of the distance d (black dots with abscissa scale on the right) between the thermal sensor and the nearest downdraft axis. (*b–f*) Successive photographs of the roll pattern in air viewed from above, $R = 9200$, at the respective times of the black dots in 6(*a*). Location of stationary thermocouple junction indicated by the black dot.

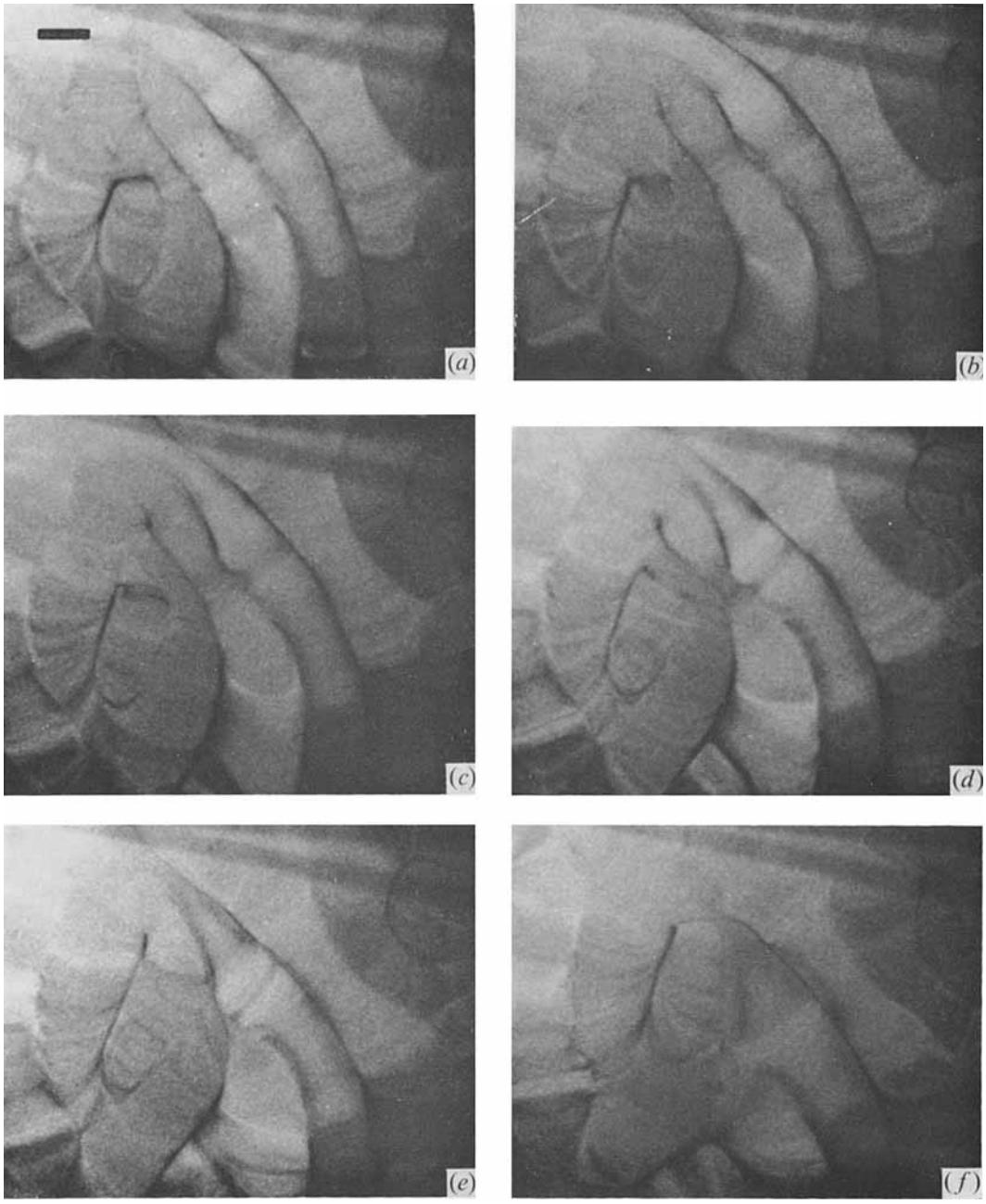

FIGURE 10. Sequence of photographs at about 8 sec intervals, showing the movement and disturbance associated with a newly formed blob or cell. $R = 4250$. Length scale in (*a*) equals chamber depth.

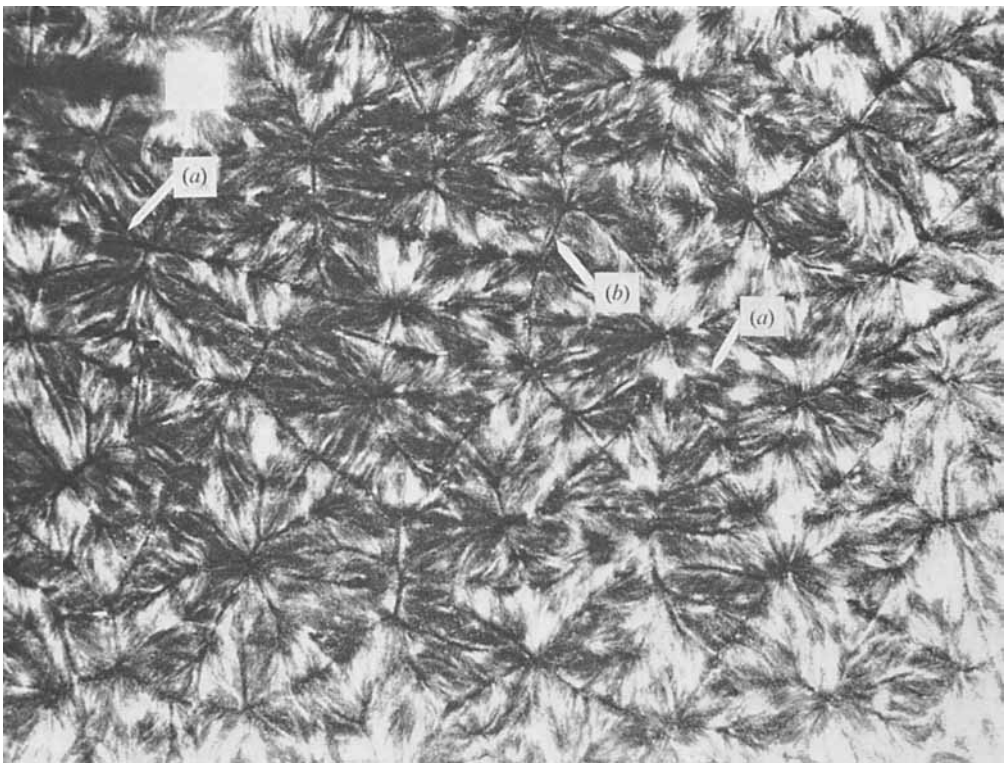

FIGURE 11. Flow patterns viewed from above during oscillations for $\sigma = 57$, $R = 4{\cdot}5 \times 10^5$. The white square has length equal to chamber depth of 1·05 cm. Labelled arrows are explained in text.